HEAT TRANSFER AND TEMPERATURE DISTRIBUTIONS IN THE FLUID AND COOLED CYLINDRICAL SOLID DURING RADIAL SLOT JET IMPINGEMENT COOLING

N Zuckerman, N Lior
University of Pennsylvania, Philadelphia, USA

Abstract

A conjugate heat transfer investigation was conducted to better understand the effects of an impinging radial slot jet cooling device on both the heat transfer rates and temperature fields in the fluid, and especially in the cylindrical solid cooled by this device. Such temperature nonuniformities in the solid are of practical interest as they may result in phenomena such as non-uniform material properties, residual thermal stresses, and distortion of the target shape, and several metrics for this nonuniformity were defined and evaluated. The study used numerical methods to model a configuration in which a set of four radially-positioned slot jets cooled a cylindrical steel target using air with a jet Reynolds number of 20,000. The steady-state v^2f RANS model was used with a representative two-dimensional section of the axisymmetric target and flow domain. The conjugate heat transfer/CFD model was run for three cases: (1) constant inner surface temperature, (2) constant inner surface heat flux, and (3) constant volumetric heat generation. The target wall thickness and thermal conductivity were varied to study lateral conduction in the solid. Heat source intensity was also varied to assess its influence. Results showed that for Biot (Bi) numbers between 0.0025 and 0.073 the temperature levels in the solid were clearly affected by lateral conduction, and that the temperature variation within the solid was an order of magnitude smaller than the variation in the surface heat transfer coefficient. Despite the relatively large temperature difference of up to 400K between the cooling fluid and the solid surface, the conduction in the solid was found to have a negligible effect on the flow and heat transfer in the fluid, and on the convective heat transfer coefficient on the solid interface. For the constant heat flux case, the area-weighted standard deviation in the solid temperature was found to correlate well with the dimensionless parameter $Z \equiv Bi \left(d / t_{eq} \right)^2$, where d is the cylinder diameter, and t_{eq} the equivalent wall thickness, and a correlation equation was developed.

Nomenclature

B	slot jet nozzle width	p_t	total pressure
Bi	Biot number = $h\,t\,/\,k$	Pr	Prandtl number
d	target diameter	q	dynamic pressure ($\rho V^2/2$)
D	nozzle diameter	q"	heat flux
h	convective heat transfer coefficient	q'''	heat generation rate, per unit volume
H	nozzle-to-target spacing (nozzle height)	r	radial position, measured from jet axis
k_c	fluid thermal conductivity	Re	Reynolds Number (= U_0D/ν for a jet)
$MAX(\nabla T)^*$	non-dimensional maximum temperature gradient magnitude	t	wall thickness
n	number of jets	t_{eq}	equivalent wall thickness
$\hat{n}$	wall-normal unit vector	T	temperature
Nu	Nusselt Number	TR1, TR2, TR3	Temperature ratio functions
p	fluid pressure	U or u	fluid velocity component
p_s	static pressure	U_0	jet initial speed, average
		v	fluid velocity
		x_i	coordinate direction

y^+	nondimensional distance from wall	Subscripts	
		amb	ambient
Z	correlation function, $Z \equiv Bi\left(d/t_{eq}\right)^2$	avg	average (area-weighted)
		i	index number for cell or direction
θ_{az}	azimuth angle	min	minimum
ν	fluid kinematic viscosity	max	maximum
ρ	fluid density	r	radial component (e.g. v_r)
σ	standard deviation function	t	turbulent (e.g. v_t)
		0	at stagnation point
		θ	azimuthal component (e.g. v_θ)

1. Introduction

The problem of heating or cooling a body with a curved surface using impinging jets is of interest in a variety of manufacturing processes and mechanical designs. Impinging jets are used for cooling and heating manufactured goods, temperature control of operating machinery, cooling of turbine blades and combustors, drying and defogging, and mass removal. Because of the resulting thinning of the boundary layer and the beneficial effect of turbulence, impinging jets may achieve desired heat transfer rates with a flow an order of magnitude lower than conventional parallel-flow heat transfer designs. The physics and applications of these devices are detailed in many papers and a number of reviews [4, 6, 8, 9, 12]. At least as important as the rates of surface heat transfer and the associated convective heat transfer coefficients for single and multiple impinging jets, that have received much attention in the literature, is the resulting temperature and heat transfer distribution in the cooled or heated solid. This temperature distribution may result in phenomena of practical interest such as non-uniform material properties, residual thermal stresses, and distortion of the target shape (cf. [4, 7]). This aspect of impingement has, in contrast, received very little attention and understanding it is the main objective of this paper.

A specific application of interest here was the cooling of a cylindrical target by surrounding it with an array of narrow slot jets aligned with the axis of the cylinder. This arrangement offers the potential to improve uniformity of heat transfer on the surface and provide high transfer rates on the entire cylinder surface. Though slot jet impingement has been studied frequently, relatively little has been published about this configuration with this particular nozzle and target combination. Our investigation was numerical. First, a literature search was conducted to understand the strengths and weaknesses of various numerical models applied to impinging jet problems, the details of which were presented by us in [10]. Next, we used several existing time-averaged turbulence models, from the common to the most advanced ones, to examine their performance in simulating jet impingement cooling of a flat target under a round jet [11], because experimental data were available for this configuration and could be used for numerical model error assessment (no suitable data were found for a cylindrical target). At the conclusion of this assessment, we selected the v^2f model as the best one from the standpoints of practicality and accuracy for further use (DNS modeling would have probably produced better results but is impractical at this time for these Reynolds numbers), and constructed numerical models of a cylindrical target under various radial slot jet configurations. That study included the fluid domain only, and calculated the effects on Nusselt number of changes in nozzle size, target curvature, number of nozzles, jet speed, and Prandtl number [11].

The information from [11], describing the convective heat transfer at the surface of a cylindrical target, was used in this paper as a boundary condition for the computation of the resulting temperature distribution within the solid target. As the solid target's interior was not a part of the earlier models, the focus of this paper is the conjugate heat transfer study of the relationship

between the target's impingement-induced local surface heat transfer coefficients (or *Nu*) and the target interior temperature distributions, as affected by heat conduction in the solid, and, in turn, of the effects of this conduction on the overall heat transfer and temperature distribution on the target surface. Specifically, we selected a jet configuration (*Re*, *H*/2*B*, *d*/*D*, *n*) and we varied the geometry and boundary conditions associated with the solid target.

Our CFD study was thus extended by a conjugate heat transfer model to calculate temperature variations within the solid cylindrical target. This was performed by selecting a jet configuration (*Re*, *H*/2*B*, *d*/*D*, *n*) and varying geometry and boundary conditions associated with the solid target.

2. Model Configuration

2.1 Governing Equations and Numerical Method

The computational model (governing equations) for the fluid domain was based, as explained above, on the v^2f model available in Fluent 6.1.22 [5]. This model employs the common eddy-viscosity model equations for mass conservation and momentum conservation, along with equations for turbulent kinetic energy, turbulence dissipation, streamwise-normal velocity variance (v^2) and an elliptic relaxation function (*f*) which modeled the effects of walls upon v^2. For brevity, the details are not listed in this paper, but they are presented in [2, 3] along with validation comparisons. The authors had previously compared the v^2f model against the experimental data set of Baughn and Shimizu [1] to assess the v^2f model accuracy. It was found that the modeling error in the local heat transfer coefficient ranged from 2% in the wall jet to 26% in the stagnation region [11]. For the test case used the total error in Nu_{avg} was 8% when averaged over the target surface. These errors were considered acceptable, especially in view of the uncertainties in the available experimental data (such as the turbulence intensity in the approaching jet), and the typical errors in practical heat transfer correlations.

The two-dimensional steady conduction model assumed constant conductivity k_c and used the elliptic-type equation

$$k_c \frac{\partial}{\partial x_i} \frac{\partial T}{\partial x_i} + q''' = 0 \qquad (1)$$

for the interior of the solid, where *q'''* represented a general heat source term in dimensions of power per unit volume (e.g. W/m^3).

Prior to use of the conjugate heat transfer model within Fluent the conduction model was tested using a cylindrical target similar to the one to be used in the conjugate heat transfer study. The numerical solution was compared to that of closed-form analytical solution and the modeling error of the conduction model was found to be less than 1%.

Steady Fluent solutions were performed using the segregated solver with implicit equations, standard pressure equations, the SIMPLE method for pressure-velocity coupling, and first-order-upwind differencing for the momentum, energy, and turbulent flow characteristics of each quadrilateral cell [5]. Under-relaxation was used for the pressure and momentum equations to provide stable convergence.

2.2 Geometric Configuration

A numerical model was developed to incorporate a steel target of wall thickness *t*, that may represent a long annular cylinder of metal being continuously cooled, as shown in Figure 1. The section of the cylinder was modeled in two dimensions, and represented a central section of a cylindrical target located within an enclosure with end walls (Figure 2). The coolant flowed within this enclosure. The mean flow velocities were constrained to a planar surface normal to the cylinder axis, and the mean velocity component in the axial direction was set as 0 (no axial flow

because the cylinder was assumed to be very long). In addition to this assumption about symmetry in the axial direction, the geometric symmetry of the cross section was used to reduce the computational domain of the problem. The number of jets (n) was set at four, and it was assumed that all four jets had the same characteristics, and thus only one jet was modeled. The symmetry of the nozzle about its own center allowed further reduction of the domain, so that for the case with four nozzles, only 45 degrees of circumference was included in the computational domain. The solution was then reflected about the center of the slot nozzle to cover 90 degrees of circumference, and then rotated about the central axis by 90, 180, and 270 degrees to fill the full 360 degrees of azimuth.
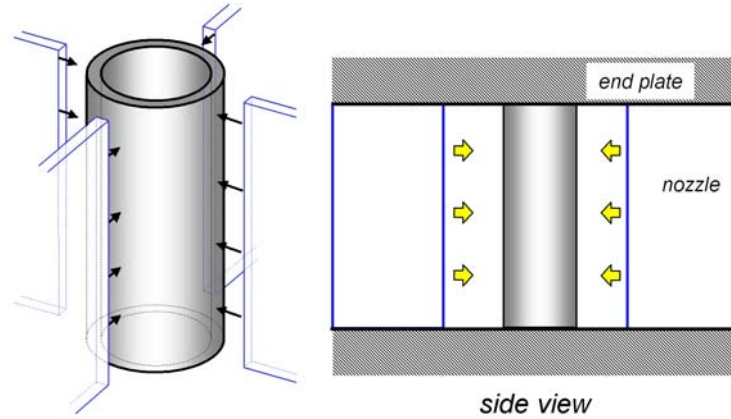
Figure 1: Isometric view and side view of target and slot jet nozzles
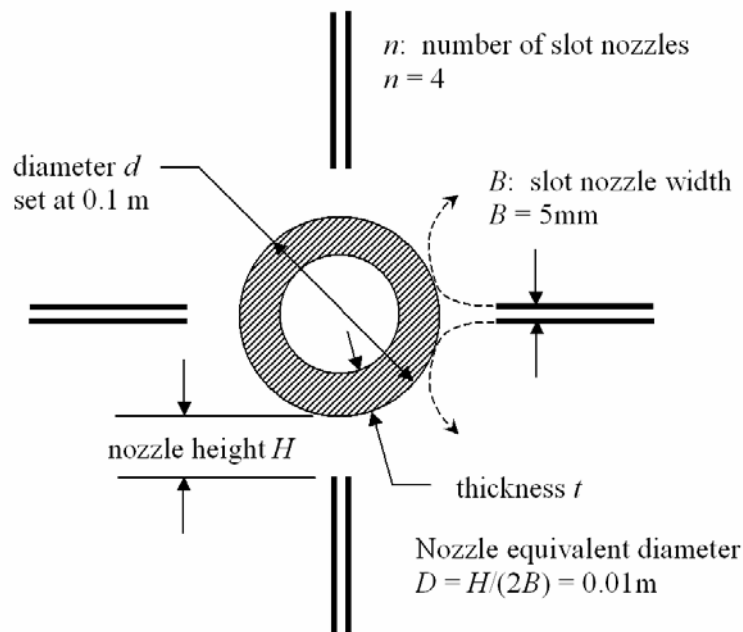
Figure 2: Model geometry for 2-dimensional section of cylindrical target

The models were constructed using structured quadrilateral grids in two dimensions. The wall grid was constructed to yield y^+ values on the order of 1 in the first wall-adjacent cell, a requirement of the v^2f model for proper resolution of the boundary layer. Cell counts were in the range of 40,000 to 120,000 cells.
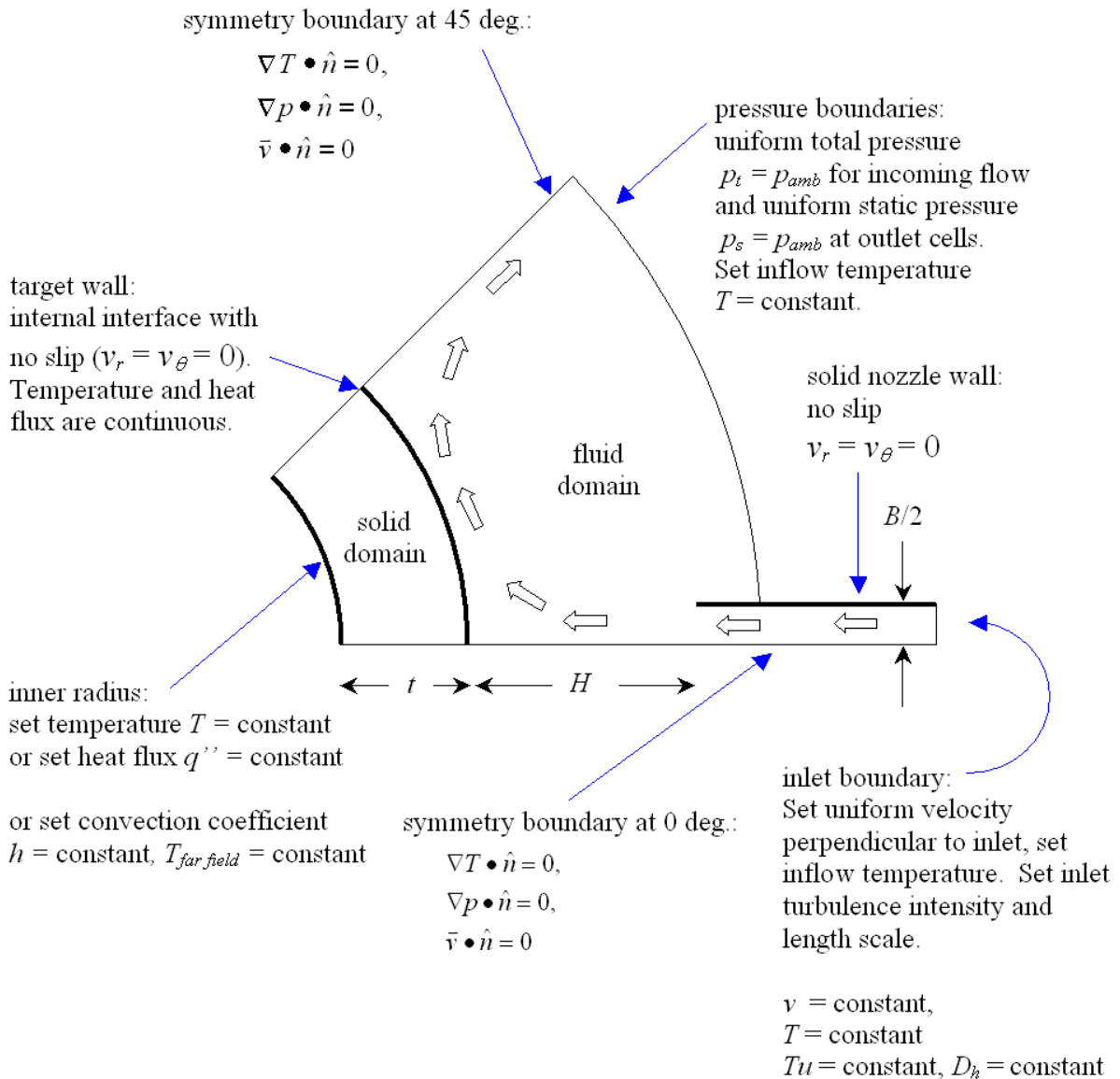
The cylinder outer diameter d was set to be 0.1 m. The ring outer radius r_o was 0.05 m and the wall thickness varied from 0.00125 m to 0.005 m. The nozzle length was set to be 0.05 m and nozzle width B was set to be 0.005 m (all are practical values for impingement cooling). The flow at the nozzle was set at 300 K and a uniform initial velocity with 1% turbulence intensity. This flow

traveled through the nozzle, with the no-slip condition at the nozzle walls, until reaching the nozzle exit. The outflow region was modeled as a constant-static-pressure boundary, allowing backflow (due possible entrainment) at a total pressure equal to the ambient static pressure.

2.3 Boundary Conditions and Material Properties

At the nozzle, the fluid temperature was assumed to be 300 K and the initial velocity uniform with 1% turbulence intensity. This flow through the nozzle was assigned a no-slip condition at the walls, until reaching the nozzle exit. The outflow region was modeled as a constant-static-pressure boundary, allowing backflow (due possible entrainment) at 300K with a total pressure equal to the ambient static pressure. The ambient pressure was set at 1 atm. As the results were correlated in a nondimensional form, the exact fluid properties were not critical to model validation.

The solid was represented as a material with uniform properties (uniform k_c) and no porosity or internal motion (velocity $v = 0$ within the solid). The energy equation used did not incorporate radiation effects, i.e. it was assumed that the temperature differences between the solid surface and the fluid were small, and the heat transfer coefficients relatively high, as they indeed were for these cases. Figure 3 shows the computational region with all boundaries and boundary conditions.

symmetry boundary at 45 deg.:
$$\nabla T \bullet \hat{n} = 0,$$
$$\nabla p \bullet \hat{n} = 0,$$
$$\bar{v} \bullet \hat{n} = 0$$

pressure boundaries:
uniform total pressure
$p_t = p_{amb}$ for incoming flow
and uniform static pressure
$p_s = p_{amb}$ at outlet cells.
Set inflow temperature
T = constant.

target wall:
internal interface with
no slip ($v_r = v_\theta = 0$).
Temperature and heat
flux are continuous.

solid nozzle wall:
no slip
$v_r = v_\theta = 0$

fluid domain

solid domain

$B/2$

inner radius:
set temperature T = constant
or set heat flux $q'' $ = constant

or set convection coefficient
h = constant, $T_{far\ field}$ = constant

symmetry boundary at 0 deg.:
$$\nabla T \bullet \hat{n} = 0,$$
$$\nabla p \bullet \hat{n} = 0,$$
$$\bar{v} \bullet \hat{n} = 0$$

inlet boundary:
Set uniform velocity
perpendicular to inlet, set
inflow temperature. Set inlet
turbulence intensity and
length scale.

v = constant,
T = constant
Tu = constant, D_h = constant

Figure 3: Computational domain for the conjugate heat transfer model

At the target surface the velocity magnitude was made zero, and, consistent with conjugate solution methods, continuity of the temperature and heat flux at the interface between the adjacent solid and fluid cells was imposed.

Constant thermal conductivities and densities were selected for the solid and fluid. The conductivity of the steel target was first set at the software default value of conductivity, k_c = 16.27 W/(m K). This value corresponded to a 26% nickel steel. To investigate the effect of the thermal conductivity of the solid, runs were also made for multiple steels with k_c from 10 W/(m K) (a 40% nickel steel) up to k_c = 73 W/(m K) (a high-purity iron). The external flow field was set at Re = 20,000, n = 4, d/D = 10. Parametric variations included type of heat source, solid material conductivity, material thickness, and heat source intensities. To examine the constant properties assumption of the air, some later studies were performed using a fluid model with temperature-dependent viscosity, conductivity, and density (ideal gas eqn.). For the range of temperatures studied, these variations changed the temperature ratios and temperature standard deviations (described below) by several percent, indicating that fluid property variation affected only the second significant figure of the results.

Consistent with the steady state assumption, three boundary conditions were assumed at the surface at the inner radius $r_i = (d/2 - t)$ of the solid: (1) constant temperature $T(r_i)$ (here set at a uniform 700 K), (2) constant heat flux (here $q'' = 100$ kW/m^2), or (3) constant heat transfer coefficient h with uniform volumetric heat generation in the solid. Both the first and second boundary conditions are possible in laboratory tests but less common in actual practice, where one expects some intermediate condition, such as an inner wall surface with small variations in temperature and larger variations in local heat flux. The two extreme conditions selected thus served to bound the problem. The third boundary condition modeled that of a heat source uniformly distributed within the solid target with an intensity of $q''' = 10$ MW/m^3 (10 W/cm^3). This could represent a target with heating due to electrical current or nuclear reaction. The inner wall of the cylinder (r_i) was set in this case at a conservative transfer coefficient of $h = 12$ W/(m^2 K) to represent mild free convection to an environment at 300 K.

Calculations were performed to assess the model grid sensitivity of the conjugate model by running the model with 74,150 cells and then by halving cell length to produce 296,600 cells. The resulting exterior wall temperature changed by 0.5 K as a result, indicating a 1.0% error due to discretization. The convergence error was found to be at least an order of magnitude smaller than the discretization error. The required computation time varied from 1 to 10 hours, using a 2 GHz Athlon 64 3200+ microprocessor running Windows XP Professional 2002 with 1 GB of RAM.
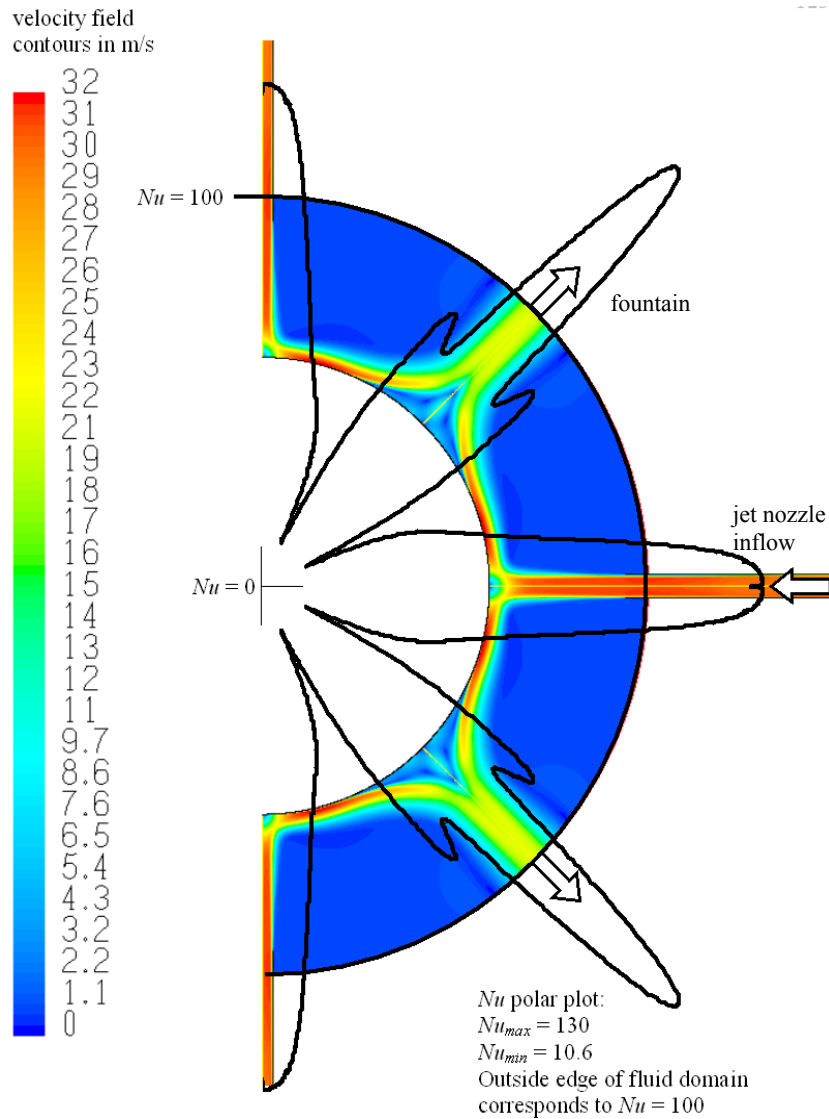
3. Results

3.1 Fluid Flow and Temperature Fields
The resulting fluid flow field is shown in Figure 4 for half of the domain. The figure also includes an overlay of the Nusselt number profile as a polar plot. The stagnation region beneath the impinging jet had a high Nu. The wall jet adjacent to the stagnation region had progressively lower Nu in the flow direction until the flow separated from the surface. Following the separation, the jet formed a fountain before exiting in a radial direction. This fountain region had only a thin boundary layer and a high Nu in the recirculating region under the fountain.

As expected the non-uniform cooling rate at the ring surface caused two-dimensional temperature nonuniformity within the wall of the annular cylinder. Figure 5 shows a typical contour map of temperature variations within sample targets with an imposed uniform heat flux of $q'' = 100$ kW/m^2 at $r_i = 0.045$ m (note the relatively narrow temperature range plotted). At a given wall thickness a

change in conductivity changed the range of temperature within the target but otherwise had small influence on the pattern of the temperature contours. A change in thickness had a clear influence on the contour map, with a reduction in thickness causing the contours to be more pronounced in the radial direction as circumferential conduction played a smaller role.

velocity field
contours in m/s

$Nu = 100$

fountain

jet nozzle
inflow

$Nu = 0$

Nu polar plot:
$Nu_{max} = 130$
$Nu_{min} = 10.6$
Outside edge of fluid domain
corresponds to $Nu = 100$

Figure 4: Fluid flow field - velocity distributions (in color) and *Nu* polar plot

3.2 Temperature Variation and Uniformity

There are various ways to express temperature nonuniformity, and their definition and utility depend on the application. The temperature data were thus reduced to four different nondimensional criteria, labeled *TR1*, *TR2*, *TR3*, and σ, to describe the temperature nonuniformity in the solid, as shown in equations (2) through (5):

$$TR1 = \frac{T_{solid\ max}}{T_{solid\ min}} \tag{2}$$

$$TR2 = \frac{T_{solid\ max} - T_{solid\ min}}{T_{solid\ max} - T_{jet}} \tag{3}$$

$$TR3 = \frac{T_{solid\ max} - T_{solid\ min}}{T_{solid\ average}} \tag{4}$$

$$\sigma = \sqrt{\frac{\sum_i A_i \left(T_i - T_{average}\right)^2}{\left(\sum_i A_i\right)\left(T_{average}^{\;2}\right)}} \tag{5}$$

The formula for *TR1* expressed the simplest of temperature ratios and incorporated no direct information about the external flow field. The equation for *TR2* showed the ratio of temperature variation within the solid to that of the entire problem, yielding a number between 0 and 1. This created a scale that incorporated the internal source effects and the cooling capability of the external flow. The equation for *TR3* represented the temperature variation in proportion to the averaged temperature, showing a percent variation in temperature.
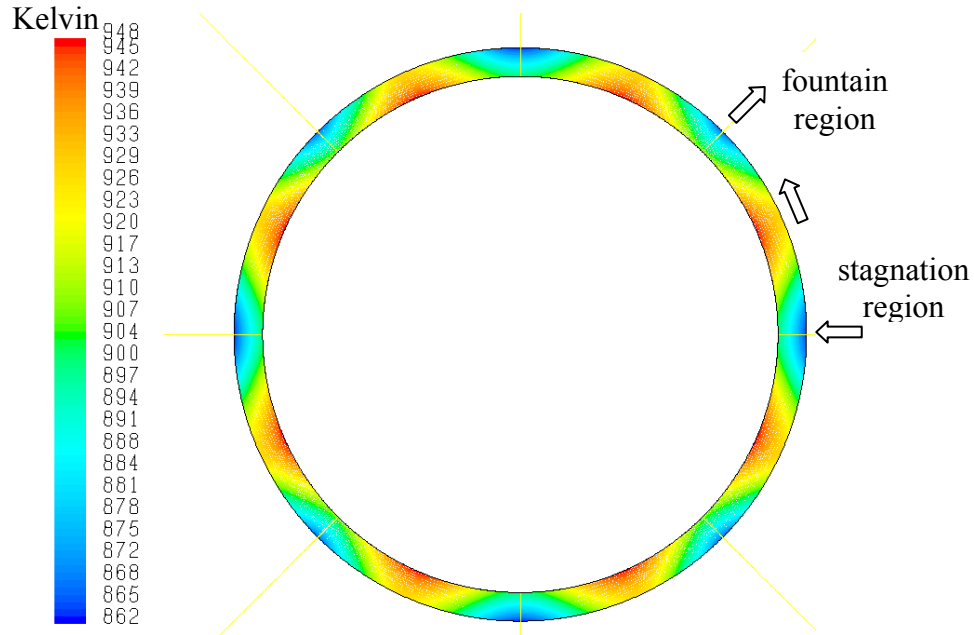
Figure 5: Typical temperature contours within the solid target in Kelvin for *t/d* = 0.05, *q''*_{inner} = 100 kW/m², *k_c* = 16.27 W/(m K)

In addition to these minimum- or maximum-based functions, the spatial extent of temperature variations within the solid were characterized using an cross-sectional-area-weighted normalized standard deviation, defined in equation (5), where A_i and T_i represented the individual cell area and cell-center temperature of each two-dimensional computational model cell. The summation was performed over all cells within the solid.

Further, the temperature gradient, which causes internal thermal stresses, was used as another nonuniformity criterion. Its distribution within the solid, and its maximum magnitude (where the highest thermal stresses may occur), were therefore computed and mapped for the cases studied. The maximum value of the gradient magnitude was nondimensionalized in the following form:

$$MAX(\nabla T)^* = MAX\left(\sqrt{\frac{\partial T_i}{\partial x_j}\frac{\partial T_i}{\partial x_j}}\right)\frac{t}{(T_{max} - T_{jet})} \tag{6}$$

The highest *T*-gradient magnitudes were found in a thin layer of the solid directly under the jet and the fountain regions where *h* was largest.

When making comparisons the wall thickness was adjusted to match that of a flat target with equivalent resistance using the equation $t_{eq} = r_{inner} \ln\left(r_{outer}/r_{inner}\right)$, where *r* represented a wall radius

of the solid. This allowed for comparison of the cooling of annular cylinders with different inner wall radii.

3.3 Influence of Parameters on Temperature Uniformity

For brevity, the complete tabular results are not presented here. Various effects of changing model parameters are summarized in Table I. Nu_{avg} varied by no more than 3% between the various cases. For all boundary conditions the maximum and average temperatures within the solid increased with an increase in source intensity [$T(r_i)$, q'', or q'''].

**Table I: Summary of the temperature ratio criteria sensitivity to parametric changes**

Variable Change	Boundary Condition	*TR1* Response	*TR2* Response	*TR3* Response
k_c increase	constant T	decrease	decrease	decrease
k_c increase	constant heat flux q''	decrease	decrease	decrease
k_c increase	constant heat generation q'''	decrease	decrease	decrease
t_{eq} increase	constant T	increase	increase	increase
t_{eq} increase	constant heat flux q''	decrease	decrease	decrease
t_{eq} increase	constant heat generation q'''	minor decrease	decrease	no change
heat source intensity increase	constant T	increase	no change	increase
heat source intensity increase	constant heat flux q''	increase	no change	increase
heat source intensity increase	constant heat generation q'''	increase	no change	increase

The first ratio examined was *TR1*. For all three boundary conditions the value of *TR1* decreased with increasing k_c, as expected. For all boundary conditions *TR1* increased with an increase in source intensity. For the constant heat flux boundary condition *TR1* decreased with increasing t_{eq}. For the constant heat generation condition *TR1* decreased slightly with increasing t_{eq}. For the constant temperature boundary condition, the effect was opposite: *TR1* increased with increasing t_{eq}. The explanation for this behavior is that increasing t_{eq} while holding inner surface temperature constant reduced the outer wall surface temperature and hence reduced the influence of the magnitude of *Nu*. For the constant temperature case, *TR1* always decreased with decreasing *Bi*. For the constant heat generation case the increase in t_{eq} raised the total heat generated as the solid volume increased, and at the same time increased the thermal resistance. These two opposing effects caused only a minor change in *TR1* with the increase of t_{eq}. For the constant heat flux boundary condition, an increase in t_{eq} caused an increase in the target thermal resistance and therefore elevated solid temperatures at the set flux.

Next the effects on *TR2* and *TR3* were examined. For all cases the values of *TR2* and *TR3* decreased with increasing k_c (as expected and also seen for *TR1*). For all three boundary conditions the value of *TR3* increased with an increase in source intensity. The value of *TR2*, however, showed no significant change with source intensity for all three boundary conditions. The *TR2* nondimensional parameter incorporated information about the full temperature scale of the problem from T_{max} to T_{jet} and was insensitive to the changes in T_{max} resulting from heat source intensity increases; *TR2* was intended to scale with source intensity. For the case with constant heat flux, the values of both *TR2* and *TR3* decreased with increasing t_{eq}. This resulted primarily from the increase in the T_{max} or T_{avg} value caused by forcing the same flux through a higher resistance. For the case of constant heat generation the value of *TR2* decreased with increasing t_{eq}, but *TR3* did not vary with

t_{eq}. The effect on *TR2* in this case resulted from scaling the model results with T_{max} while the increase in thickness lowered the relative value of T_{min}. The minimal effect on *TR3* was attributed to the competing influences of higher resistance and higher total power generation. For the constant temperature boundary condition the values of *TR2* and *TR3* both increased with increasing t_{eq}. This case was once again the opposite of the constant heat flux boundary condition, so increasing *t* at a given T_{max} produced a higher temperature drop through the target, allowing a lower T_{min} on the surface due to the increased relative influence of external convection (higher *Bi*).

For all cases an increase in k_c decreased the maximum gradient intensity, as expected. The method of nondimensionalizing the gradient magnitude made it invariant to source intensity. For all three boundary conditions the magnitude of the maximal gradient increased with increasing t_{eq}. For the majority of cases t_{eq} was within a few percent of *t*. Comparisons between models were performed using the Biot number defined as $Bi = h\, t_{eq} / k_{c\ solid}$. Given the high conductivity of the metal target, the range of *Bi* for this application was 0.0025 - 0.073. As a result, lateral conduction played an important role in smoothing out temperature variations in the solid. This effect is illustrated by the example profiles of *T* and *Nu* on the outer surface for the constant heat flux boundary condition, shown in Figure 6 for an example case with wall thicknesses $t/d = 0.05$. A comparable effect is seen in Figure 7 which shows inner and outer wall temperatures for the constant temperature boundary condition at wall thicknesses $t/d = 0.05$ and $t/d = 0.025$. As the value of *t* increased and the outer surface temperature minima decreased, the regions of peak outer surface temperature also shifted farther away from the stagnation region.
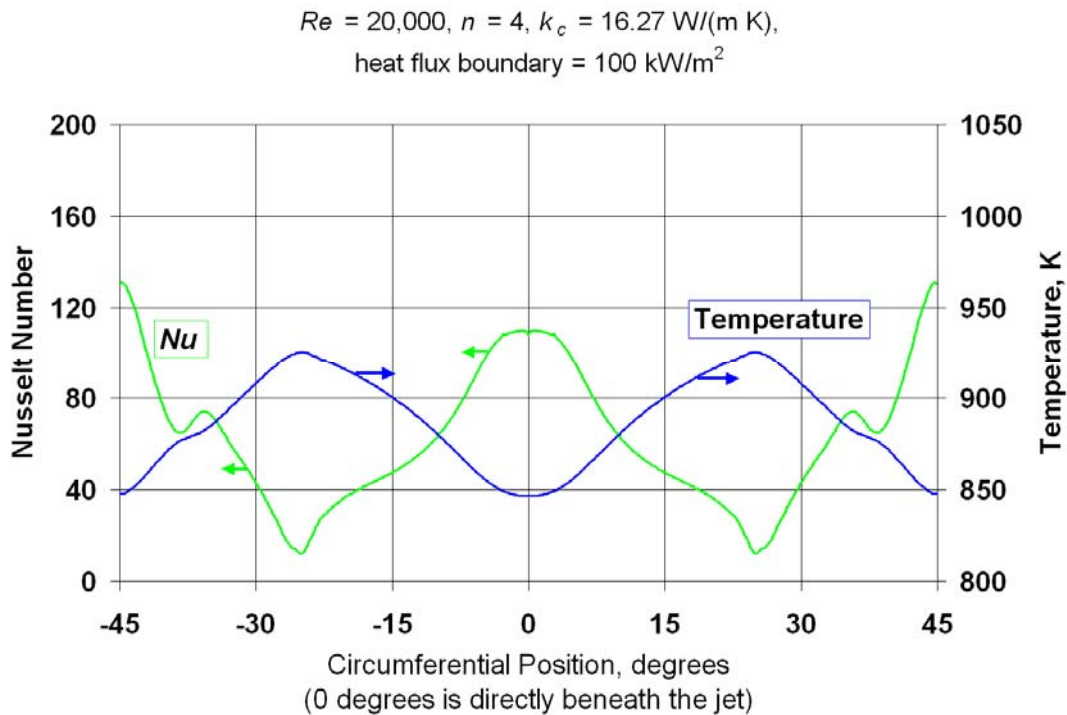
Figure 6: Nusselt Number and Temperature profiles on outer surface for $t/d = 0.05$, $q''_{inner} = 100\ \text{kW/m}^2$, $k_c = 16.27$ W/ (m K)

Even though the local *Nu* varied by a factor of ten, the temperature variations in the solid were in the range of one-quarter to one-tenth of the overall temperature range in the problem. The regions of high fluid temperature (within 10% of the wall temperature) occupied only a small portion of the fluid volume within the computational domain boundary as the heat rapidly dropped off within the thermal boundary layer. The resulting *Nu* profile for the conjugate problem was very close to that found in the case of zero wall thickness [11], with variations in *Nu* between cases in the studied range of only 1-3%. This showed that, within the range of variable values considered, conduction

in the solid in the analysis has a negligible effect on the flow and heat transfer in the fluid, and on the convective heat transfer coefficient on the solid interface. One practical conclusion is that it is not necessary to consider the conjugate problem if only the fluid dynamics and heat transfer in the fluid are of interest.
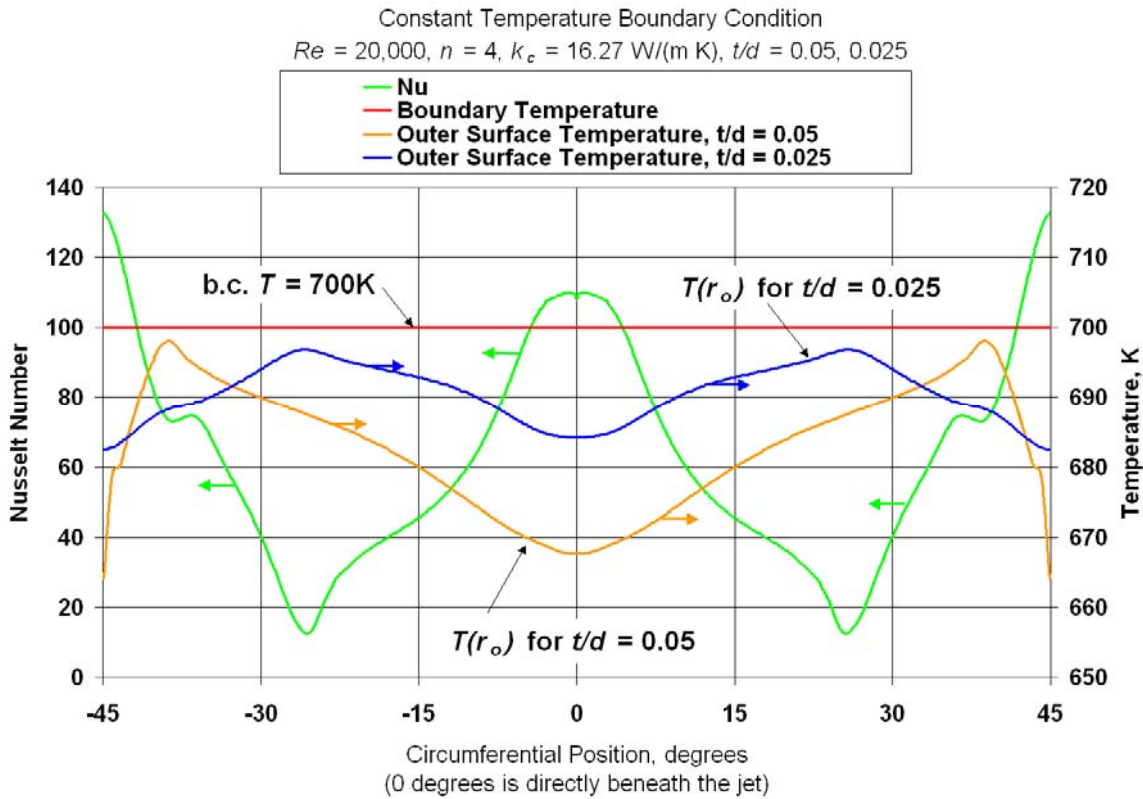
Figure 7: Nusselt Number and Temperature profiles on outer surface for *t/d* = 0.05 and 0.025, $T(r_i)$ = 700 K, k_c = 16.27 W/ (m K)
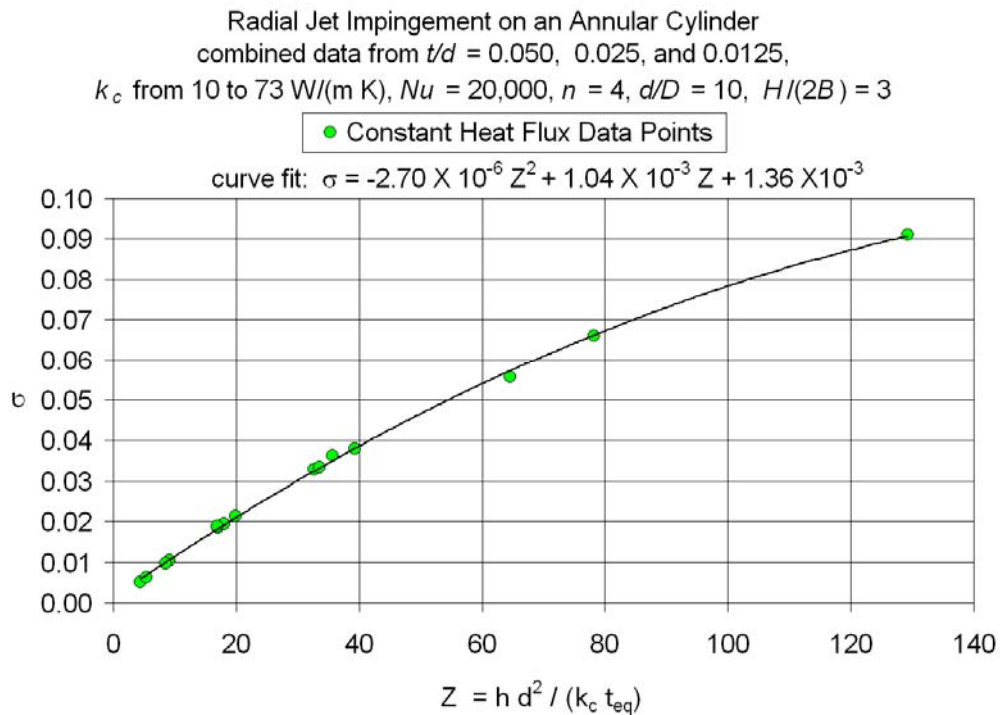
The Biot number *Bi* serves a useful purpose in describing the expected temperatures in the target. Further examination of the influence of k_c and *t* upon the heat distribution led to the conclusion that parameters describing uniformity of temperature did not and should not correlate with *Bi*, if we define *Bi* as $Bi = \dfrac{ht_{eq}}{k_c}$. In general the Biot number described the relative importance or strength of external convective transfer rate (*h*) to internal conductive heat transfer (k_c / t_{eq}). It did not incorporate any direct information regarding the uniformity within the target. To explain, as k_c is increased, and hence *Bi* decreased, it would be expected to obtain a more uniform temperature field within the solid target. Yet if *t* was increased, and *Bi* thus increased, it would also be expected to see a more uniform temperature within the target. So, a highly uniform temperature field could be associated with either high or low *Bi*, meaning *Bi* alone does not provide information allowing one to draw a conclusion about the expected temperature uniformity.

As stated above, the uniformity of the temperature was expected to increase both with increasing k_c and with increasing t_{eq}. Based on this relationship, a new non-dimensional parameter was selected:

$$Z = \frac{h(d^2)}{kt_{eq}} = Bi\left(\frac{d}{t_{eq}}\right)^2 \tag{7}$$

Because of the varying lateral conduction effects for the cylindrical geometry at different nondimensional thicknesses (*t/d*), the value of thickness *t* used in the *Z* equation was the equivalent flat-plate thickness t_{eq}.

Comparison of σ values vs. Z for different k_c and t using the constant heat flux boundary condition showed a successful correlation with all points falling on a single curve. One should note that the influence of variations in h and the nonuniformity of the h profile upon σ were not investigated in this study. For this reason the inclusion of h in the numerator was for convenience only; further studies should more thoroughly define the functional dependence on h (and thus k, t, n, Re, and t/d) and redefine the form of Z. Future work could then produce a new form of the Z function which would incorporate all of these independent variables, replacing h with another function, perhaps in a form incorporating both h_{max} and h_{min}. The σ data for the other two boundary conditions did not correlate well with the form of Z shown in eqn. (7). It is likely that with more parameters incorporated into the Z function it can be reformulated for problems with all three boundary conditions. Figure 8 shows the trend of σ vs. Z for the constant heat flux boundary condition.

Radial Jet Impingement on an Annular Cylinder
combined data from t/d = 0.050, 0.025, and 0.0125,
k_c from 10 to 73 W/(m K), Nu = 20,000, n = 4, d/D = 10, $H/(2B)$ = 3

● Constant Heat Flux Data Points

curve fit: $\sigma = -2.70 \times 10^{-6} Z^2 + 1.04 \times 10^{-3} Z + 1.36 \times 10^{-3}$

Figure 8: Standard Deviation of Temperature σ vs. Z for t/d = 0.050, 0.025, and 0.0125, k_c from 10 to 73 W/(m K)

4. Conclusions

A conjugate heat transfer study of the effects of multiple (4) axial slot cooling jet impingement on a hot long cylindrical pipe was conducted. The study examined the temperature distributions and nonuniformities in the solid cylinder wall for Re = 20,000, 10 W/(m K) $\leq k_c \leq$ 73 W/(m K), 0.0125 $\leq t/d \leq$ 0.0500, 0.0025 $\leq Bi \leq$ 0.073, and 4.4 $\leq Z \leq$ 129. Despite the relatively large temperature difference of up to 400K between the cooling fluid and the solid surface, the conduction in the solid was found to have a negligible effect on the flow and heat transfer in the fluid, and on the convective heat transfer coefficient on the solid interface. One practical conclusion is that it is not necessary to consider the conjugate problem if only the fluid dynamics and heat transfer in the fluid are of interest.

For the constant heat flux boundary condition on the internal pipe surface, the dimensionless parameter $Z \equiv Bi\left(d/t_{eq} \right)^2$ was found to correlate well the internal temperature nonuniformity

standard deviation σ with the values of k_c and t/d in that range. Defining and using several nonuniformity evaluation criteria, we found initial indications of the importance of lateral conduction in an annular cylinder cooled by radial impinging jets. For the cases studied herein, the lateral conduction played an important role in making the temperature nonuniformity in the solid an order of magnitude smaller than the nonuniformity in the surface Nu caused by the impinging jets.

Acknowledgements

References

1.   Baughn, J.W. and Shimizu, S., 1989, Heat Transfer Measurements from a Surface with Uniform Heat Flux and an Impinging Jet, ASME Journal of Heat Transfer, 111, 1096-1098.
2.   Durbin. P. A., 1993, A Reynolds Stress Model for Near-wall Turbulence, Journal of Fluid Mechanics, 249, 465-498.
3.   Durbin, P., 1995, Separated Flow Computations with the k-ε-v² Model, AIAA Journal, 33, 659-664.
4.   Ferrari, J., Lior, N., and Slycke, J., 2003, An Evaluation of Gas Quenching of Steel Rings by Multiple-Jet Impingement, J. Materials Processing Technology, 136, 190-201.
5.   Fluent Inc., 2003, Fluent 6.1 User's Guide, 01-25-2003.
6.   Jambunathan , K., Lai, E., Moss, M. A., and Button, B. L., 1992, A Review of Heat Transfer Data for Single Circular Jet Impingement, International Journal of Heat and Fluid Flow, 13, 106-115.
7.   Lior. N., 2004, The Cooling Process in Gas Quenching, Journal of Materials Processing Technology, 155-156, 1881-1888.
8.   Martin, H., 1977, Heat and Mass Transfer between Impinging Gas Jets and Solid Surfaces, Advances in Heat Transfer, 13, 1-60.
9.   Viskanta, R., 1993, Heat Transfer to Impinging Isothermal Gas and Flame Jets, Experimental Thermal and Fluid Science, 6, 111-134.
10.   Zuckerman, N., and Lior, N., 2005, Impingement Heat Transfer: Correlations and Numerical Modeling, ASME Journal of Heat Transfer, 127, 544-552.
11.   Zuckerman, N.., and Lior, N., 2005, Jet Impingement Heat Transfer on a Circular Cylinder by Radial Slot Jets, Proceedings of IMECE05, 2005 ASME International Mechanical Engineering Congress and Exposition, November 5-11, Orlando, Florida, USA.
12.   Zuckerman, N., and Lior, N., 2006, Jet Impingement Heat Transfer: Physics, Correlations, and Numerical Modeling, Advances in Heat Transfer vol. 39, chapter in press.